Electron. Mater. Lett., Vol. 10, No. 1 (2014), pp. 61-65
DOI: 10.1007/s13391-013-3039-9

Growth and Characterization of $Mg_xZn_{1-x}O$ Thin Films by Aerosol-Assisted Chemical Vapor Deposition (AACVD)

Akash Shukla,[1] Vipin K. Kaushik,[2] and Dixit Prasher[1,*]

[1]Rawal Institute of Engineering & Technology, Faridabad, 121001, India
[2]Department of Applied Physics, Shri G.S. Institute of Technology and Science, Indore, 452003, India

(received date: 24 February 2013 / accepted date: 26 March 2013 / published date: 10 January 2014)

The growth and characterization of $Mg_xZn_{1-x}O$ thin films by aerosol-assisted chemical vapor deposition (AACVD) technique is reported in this paper. We have grown the thin films of ZnO by adding varying concentrations of magnesium (Mg) on a glass substrate. The precursor from which the $Mg_xZn_{1-x}O$ thin films were grown was made up of a mixture of zinc acethylacetonate and magnesium acetate tetrahydrate in boiled isopropyl alcohol. Oxygen gas was used as a carrier gas and substrate temperature was maintained at 400°C. $Mg_xZn_{1-x}O$ thin films were finally characterized by x-ray diffraction (XRD), atomic force microscopy (AFM) and UV-VIS-NIR spectroscopy. XRD results show that $Mg_xZn_{1-x}O$ thin films displayed a wurtzite structure and addition of Mg leads to a slight shift towards higher 2-theta values. AFM results show that MgZnO thin films were uniformly covered with nano flakes and their size decreases with an increase in Mg content. Optical studies show that with the increase of Mg content, transparency as well energy band gap of the $Mg_xZn_{1-x}O$ thin films increases, which also agrees with the reported values.

Keywords: ZnO, $Mg_xZn_{1-x}O$, MgZnO, thin films, CVD, XRD

1. INTRODUCTION

Zinc oxide (ZnO) is a leading *II-VI* semiconductor with a wide direct-band gap (3.37 eV) and high cohesive energy (1.89 eV). It has attracted much attention over the past years because of its wide applications in thin film transistors, organic light emitting diodes, ultraviolet optoelectronic devices, gas sensors, solar cells, etc.[1-5] It is found that doping in ZnO affects the electrical properties of ZnO thin films as the dopant atom replaces the host Zn atoms, which leads to a change in conductivity, room temperature ferromagnetism and sensing character.[6] Zinc oxide-based alloys have also attracted research interest during the past few years. These alloys include $Mg_xZn_{1-x}O$, which could produce a bright ultraviolet luminescence at room temperature due to the band edge exciton recombination. This renders MgZnO alloy thin films very good materials for use as optoelectronic devices.[7] It was also reported that Mg-doped ZnO gained much interest in the field effect transistors for its hydrogen storage behavior.[8-10] The major interest in this alloy is mainly from the consideration of band gap engineering. Band gap of ZnO can be increased by alloying it with magnesium oxide, which has a band gap of 7.7 eV, and decreased by alloying it with cadmium oxide having a band gap of 2.3 eV.[11-14] Another reason for synthesizing such ZnO-based alloys is to construct superlattice heterostructures with less lattice-mismatched alternative layers such as ZnO/$Mg_xZn_{1-x}O$. Many efforts have been made to grow high-quality ZnO thin films using various deposition techniques such as sol-gel method, spray pyrolysis, pulsed laser deposition (PLD), and also using magnetron sputtering.[15-18] However, AACVD has the advantage of constructing devices on a commercial scale because of its high deposition rate and high crystallinity. The technique requires lower deposition temperature for the deposition of thin film on a polymer-like substrate. It simplifies the vapor generation and delivery method as compared to the conventional CVD method.

2. EXPERIMENTAL PROCEDURE

The $Mg_xZn_{1-x}O$ thin films were deposited on a glass substrate by aerosol-assisted chemical vapor deposition (AACVD) technique. The precursor from which the MgZnO thin films were grown was made up of a mixture of zinc acethylacetonate and magnesium acetate tetrahydrate in boiled isopropyl alcohol. Oxygen gas was used as a carrier gas and substrate temperature was kept at 400°C. The precursor, in the form of aerosol, under the huge pressure of carrier gas reaches up to the heated substrate where it chemically combines with Zn and Mg to form $Mg_xZn_{1-x}O$ and gets deposited on to the substrate surface. The chemical reaction taking place in reaction zone is shown as follows:

*Corresponding author: dixit.prasher@gmail.com

$(C_5H_7O2)_2Zn.H_2O + (CH_3COO)_2Mg + C_3H_7OH =$
$Mg_xZn_{1-x}O$ + gaseous product.
(Zinc acethylacetonate) (magnesium acetate tetrahydrate)

In the beginning of this process, isopropyl alcohol is boiled up to its boiling temperature. The precursor of ZnO (zinc acethylacetonate) added dropwise to the boiled isopropyl alcohol. The formed solution is again boiled with continuous stirring until the solution becomes transparent. The source of MgO (magnesium acetate) is added dropwise to the prepared solution with stirring until the particles are completely dissolved in the solution. After preparing the final solution, it is sprayed onto the heated substrate with the help of a carrier gas. When the substrate temperature reaches the desired growth temperature, oxygen gas along with the precursor solution is allowed to pass through the fine nozzle jet where the precursor gets converted into an aerosol. At the same time O_2 is used as a carrier gas to guide the formed aerosol inside the reactor. The substrate, now in the form of aerosol, under the huge pressure of carrier gas reaches the heated substrate where it chemically combines with Zn and Mg to form $Mg_xZn_{1-x}O$ and is deposited onto the substrate surface. The unconsumed gases are vented out of the reactor in order to provide a free flow of the precursor and carrier gas. After the complete flow of the precursor solution through the reaction chamber, the substrate is ejected out from the chamber and subjected to different characterizations to analyze the quality of deposition. For preparing the aerosol, the reaction chamber pressure of gas to which the precursor solution flows is set at 0.1 - 0.5 bar and the substrate temperature is maintained at a constant value of 200°C - 400°C. The nozzle to substrate distance and diameter of nozzle is set at 450 mm and 0.5 mm, respectively. Structural studies of the films were performed using a Philips D8 advanced x-ray diffractometer. Cu-K_α radiation was used in the XRD studies. The atomic force microscopy (AFM) studies were performed on Nanoscope V Dimension 3010 AFM3. Optical studies were carried out on Shimadzu-1700 UV-VIS-NIR spectrophotometer.

3. RESULTS AND DISCUSSIONS

Figure 1(a), 1(b) and 1(c) shows the x-ray diffraction patterns of pure ZnO and $Mg_xZn_{1-x}O$ thin films when (a) 'x' = 0, (b) 'x' = 0.15, (c) 'x' = 0.3 grown on glass substrate at 400°C temperature. The XRD pattern of the grown samples supports the polycrystalline nature of the deposition. This may be due to the polycrystalline nature of glass itself. However, a strong preferential (002) orientation has been detected for both of the samples, which is presumably due to the amorphous nature of glass and the formation of an amorphous zinc oxide layer on the substrate. In Fig. 1(a), several strong peaks occur at $2\theta = 31.86°$, $2\theta = 34.49°$, $2\theta = 36.36°$, which respectively correspond to (100), (002), (101) diffraction planes of the hexagonal ZnO. In Fig. 1(b) some other peaks are also found in the 2θ angles of 56.4°, 62.8° and 67.9° corresponds to (103), (200) and (112) planes of the wurtzite structure, respectively. The strong peak occurring at $2\theta = 41.86°$ and $2\theta = 36.86°$ in Fig. 1(c) corresponds to the presence of MgO (200) and amorphous Mg_3Zn_7O (002) diffraction planes in the deposition. It was observed that there is a slight shift in the 2θ values, which is due to the decrease in lattice spacing caused by the incorporation of Mg content into the Zn lattice.

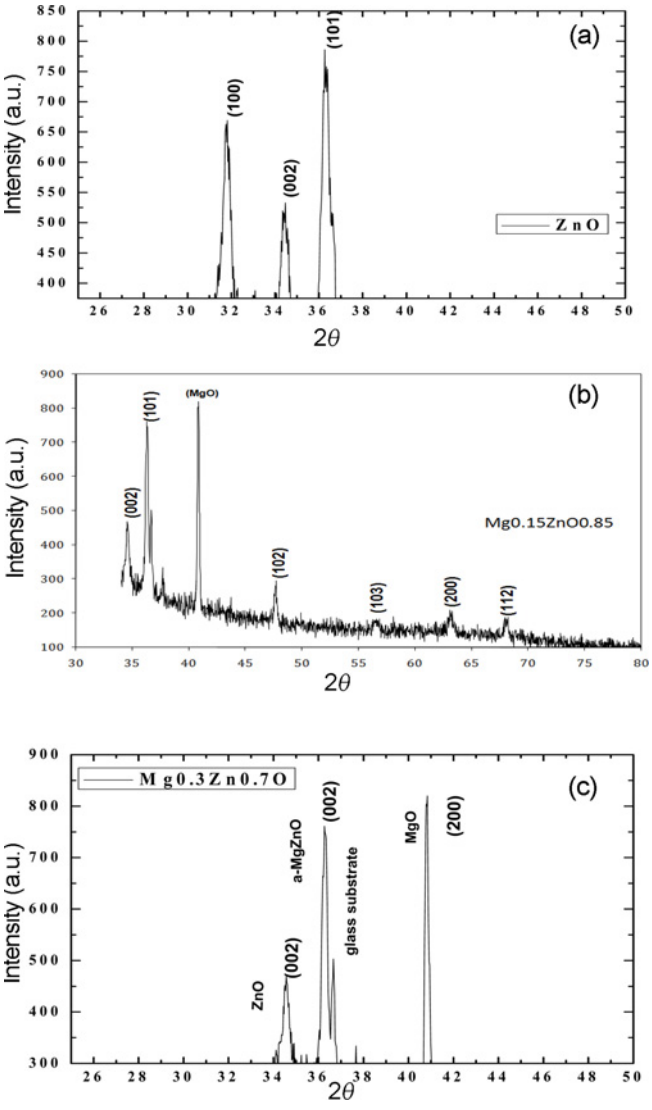

Fig. 1. (a), (b), (c) XRD patterns of Mg doped ZnO thin film when (a) 'x' = 0, (b) 'x' = 0.15, (c) 'x' = 0.3 grown on glass substrate at 400°C temperature.

Surface morphology of the Mg-doped ZnO films was studied by atomic force microscopy. Figure 2(a) and 2(b) shows the AFM 2D micrographs with their 3D images of the $Mg_xZn_{1-x}O$ thin films where x = 0.1 and 0.3, respectively. It

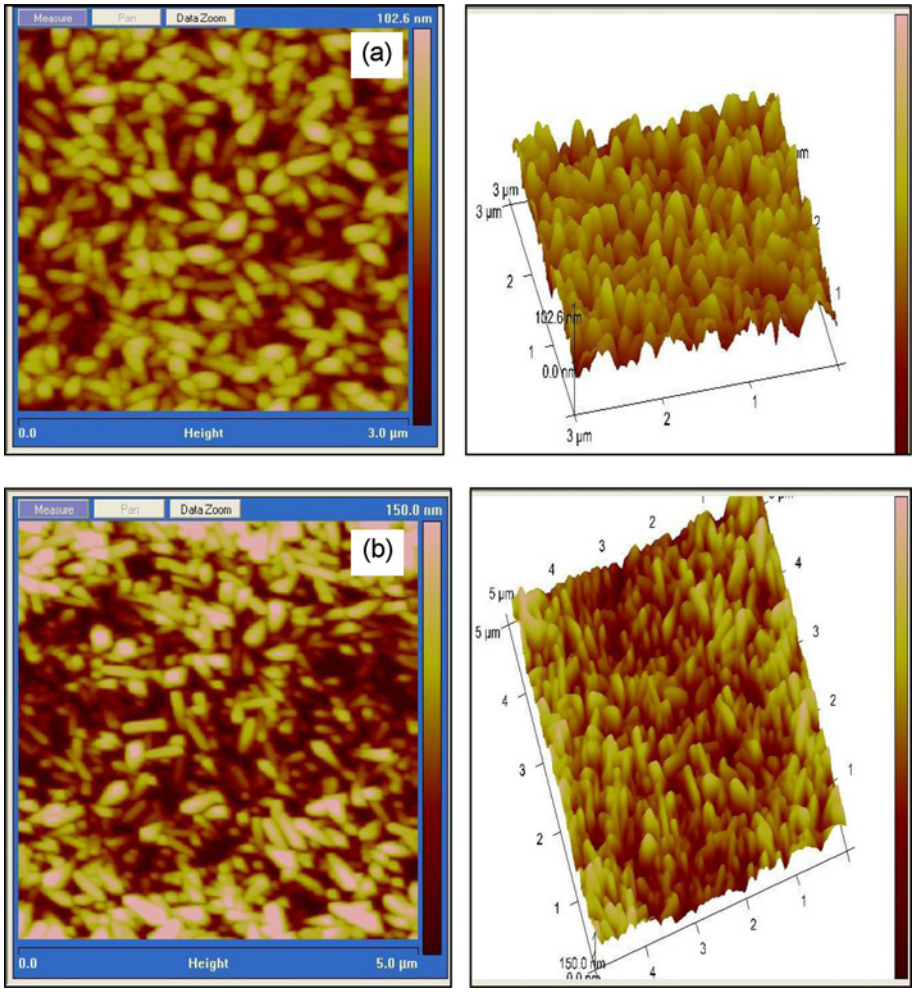

Fig. 2. (a) and (b) show the AFM 2D micrographs with their 3D images of the $Mg_xZn_{1-x}O$ thin films when 'x' = 0.1 and 'x' = 0.3, respectively.

can be clearly seen from Fig. 2 that both the films are uniformly covered with nano flakes and that as the Mg concentration increases, the morphology of the ZnO films drastically changes, as evident by the grains being smaller in size. In the present work we also calculated the average value of roughness of the films through AFM, which was found to be 14.0 and 34.1 nm for x = 0.1 and 0.3, respectively. Morphological studies for some of the samples were also carried out by using scanning electron microscope. Figure 3(a), 3(b) and 3(c) shows the SEM micrographs of Mg doped ZnO thin film when (a) 'x' = 0.05, (b) 'x' = 0.15 (c) 'x' = 0.2 grown on glass substrate at 400°C temperature. It can be clearly seen that all samples are uniformly covered with nano flakes (Fig. 3(a), 3(b)) and spherical shape nano grains (Fig. 3(c)).

Figure 4 presents the plots of the absorption coefficient versus photon energy. This curve clearly shows the excitonic nature of absorption spectra for x = 0.0, 0.05, 0.1, 0.15, 0.2 and 0.3. Since the excitonic binding energy of $Mg_xZn_{1-x}O$ is almost the same as that of ZnO (60 MeV) the excitonic peak is present for all the films with x = 0.0, 0.05, 0.1, 0.15, 0.2 and 0.3. When Mg is substituted in ZnO, an equilibrium solid solution is formed up to x = 0.05 in accordance with the thermodynamical solubility limit. For $0.05 \leq x \geq 0.20$, a non-equilibrium solid solution is formed displaying compositional nonuniformity. This leads to generation of nonequilibrium compensated defects, which is reflected in sudden changes in the electrical and optical properties of the films. Considering the excitonic effect, band gap values (for band to band transition) for $Mg_xZn_{1-x}O$ thin films have been calculated and plotted as shown in Figure 5. The optical band gap was estimated from the linear intercept of the $(\alpha h\nu)^2$ versus $h\nu$ plots. The obtained optical band gap energy for pure ZnO is 3.27 eV. This value is slightly lower than that of bulk ZnO (i.e. 3.31 eV) and in good agreement with the previously reported data for ZnO thin films. The value increases linearly from 3.27 eV for x = 0.0–3.54 eV for x = 0.3. There is a shift in the energy band gap, which is due to the assimilation of Mg into ZnO lattice and agrees with the reported values. Beyond this composition value, band gap

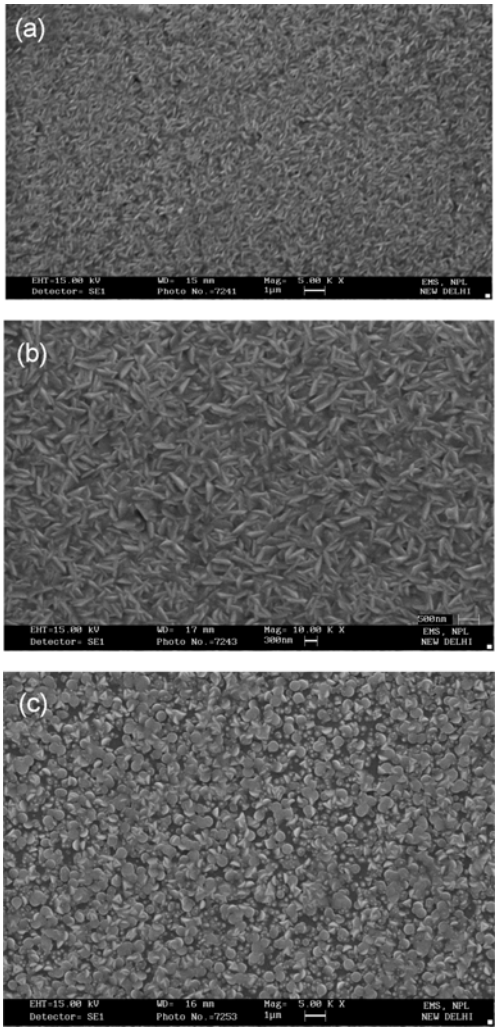

Fig. 3. (a), (b), (c) SEM micrographs of Mg doped ZnO thin film when (a) 'x' = 0.05, (b) 'x' = 0.15, (c) 'x' = 0.2 grown on glass substrate at 400°C temperature.

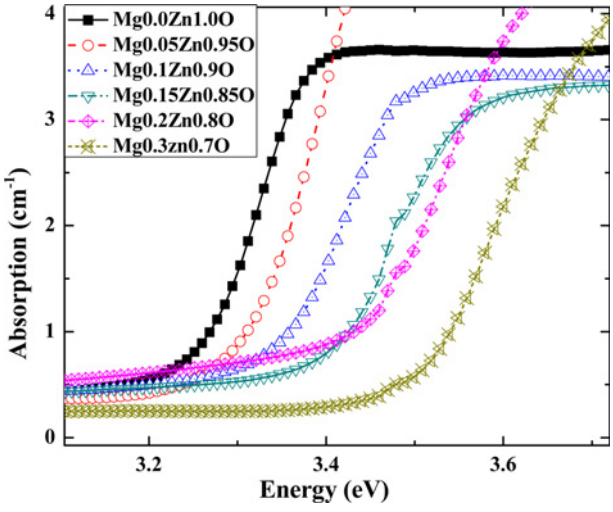

Fig. 4. Variation of optical absorbance coefficient of $Mg_xZn_{1-x}O$ thin films with the incident photon energy.

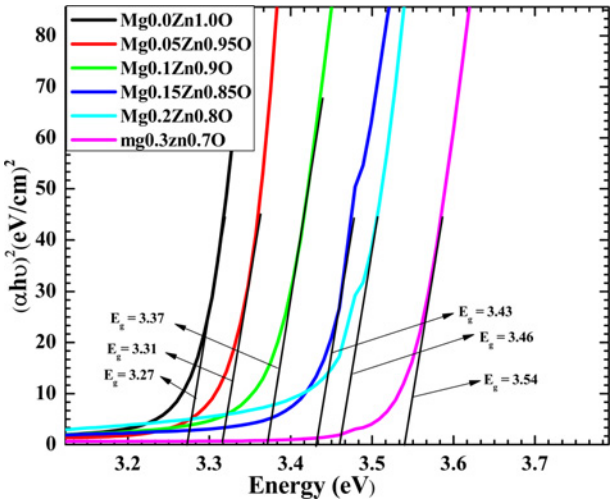

Fig. 5. Plot of $(\alpha h\nu)^2$ as a function of photon energy (eV) for the $Mg_xZn_{1-x}O$ thin films.

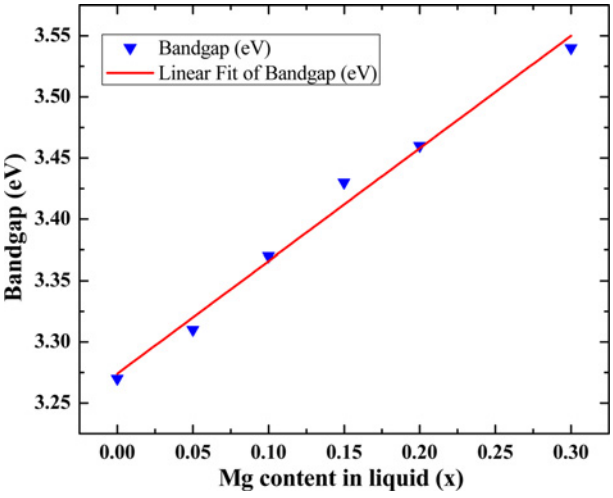

Fig. 6. Variation of band gap (E_g) with Mg content (x) in liquid solution of $Mg_xZn_{1-x}O$. The solid line represent the linear fit of the corresponding data from $x = 0$ to $x = 0$ .3.

values are irregular. The slope of variation of band gap up to $x = 0.05$ is lower than those reported earlier. The lower experimental values of Mg:Zn ratio might explain the lower band gap values in the present $Mg_xZn_{1-x}O$ thin films. The linear variation of band gap with magnesium content from $x = 0$ to $x = 0.3$ is shown in Fig. 6. The linear nature of this curve reflects that the probability of further incorporation of Mg in the lattice site of ZnO still exists. Since the maximum value of band gap obtained for our depositions is around 3.53 eV at 0.1 mol. % of Mg in solid film, which corresponds to the hexagonal structure of MgZnO maintained in our last deposition. Figure 7 shows the transformation of Mg from a liquid solution to the final solid deposition in our system. The linear nature of this curve reflects the fact that larger the

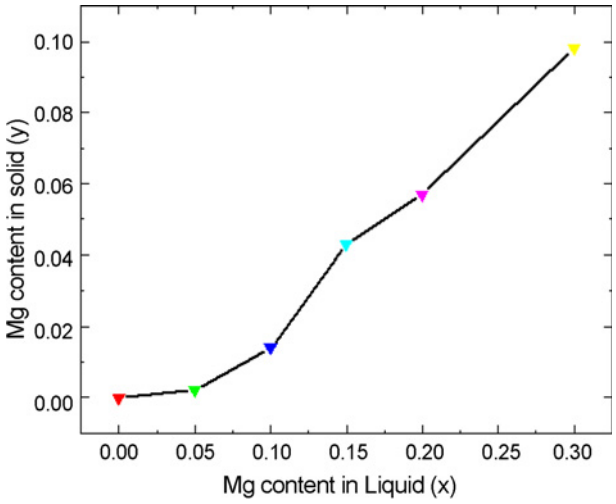

Fig. 7. The variation of 'Mg' mole fraction (%) in solid with respect to the 'Mg' mole fraction (%) in liquid.

value of Mg precursor in the solution larger the Mg content in the solid film.

4. CONCLUSIONS

We have shown in this work that high-quality polycrystalline MgZnO films can be grown on glass substrates by using aerosol-assisted chemical vapor deposition method. Mg content achieved by our growth system is almost an order of magnitude higher than that predicted by the reported results. The optical band gap has been increased from 3.2 to 3.5 eV by adjusting the Mg content. Throughout this tuning range, the crystal quality was sufficiently preserved to maintain the hexagonal crystal structure of the material, which has been confirmed by the XRD pattern of the samples. The amorphous phase in ZnO films obtained in films deposited at a slightly highly temperature is believed to be the main reason for the blueshift of optical band gap. These results provide important information for the design and modeling of ZnO/MgZnO heterostructure optoelectronic devices. The ability to grow high-quality MgZnO alloy films opens up numerous possibilities for the construction of ultraviolet optoelectronic devices.

ACKNOWLEDGMENTS

We are thankful to NPL, Delhi, and RRCAT, Indore, India, for providing the AFM, XRD, UV-VIS-NIR facilities.

REFERENCES

1. J. H. Kim, B. D. Ahn, C. H. Lee, K. A. Jeon, H. S. Kang, and S. Y. Lee, *Thin Solid Films* **516**, 1529 (2008).
2. Y. Xia, P. Yang, Y. Sun, Y. Wu, B. Mayers, and B. Gates, *Adv. Mater.* **15**, 353 (2003).
3. N. Kumar, A. Dorfman, and J. Hahm, *Nanotechnology* **17**, 2875 (2006).
4. Z. P. Sun, L. Liu, L. Zhang, and D. Z. Jia, *Nanotechnology* **17**, 2266 (2006).
5. D. Banerjee, S. H. Jo, and Z. F. Ren, *Adv. Mater.* **16**, 2028 (2004).
6. J. Liu and X. Huang, *J. Solid State Chem*. **179**, 843 (2006).
7. R. Ding, C. Xu, B. Gu, Z. Shi, H. Wang, and Z. Xiao, *J. Mater. Sci. Technol.* **26**, 601 (2010).
8. S. Ju, J. Li, N. Pimparkar, M. A. Alam, R. P. H. Chang, and D. B. Janes, *IEEE T Nanotechnol.* **6**, 390 (2007).
9. Q. Wan, C. L. Lin, X. B. Yu, and T. H. Wang, *Appl. Phys. Lett*. **84**, 124 (2004).
10. H. Pan, J. Luo, H. Sun, Y. Feng, C. Poh, and J. Lin, *Nanotechnology* **17**, 2963 (2006).
11. C. X. Cong, B. Yao, Q. J. Zhou, and J. R. Chen, *J. Phys. D: Appl. Phys*. **4**, 105303 (2008).
12. T. Gruber, C. Kichner, R. Kling, F. Reuss, A. Waag, and F. Bertram, *Appl. Phys. Lett*. **83**, 3290 (2003).
13. G. H. Ning, X. P. Zhao, and J. Li, *Opt. Mater*. **27**, 1 (2004).
14. K. Ellmer and G. Vollweiler, *Thin Solid Films* **104**, 496 (2006).
15. R. Kaur, A. V. Singh, K. Sehrawat, N. C. Mehra, and R. M. Mehra, *J. Non-Cryst. Solids* **352**, 2565 (2006).
16. B. Godbole, N. Badera, S. Shrivastava, D. Jain, and V. Ganesan, *Mater. Sci. Appl*. **2**, 643 (2011).
17. J. Zippel, S. Heitscha, M. Stolzela, A. Mullera, H. Wencksterna, and G. Benndorfa, *J. Lumin*. **130**, 520 (2010).
18. J. B. Lee, H. J. Kim, S. G. Kim, C. S. Hwang, S. H. Hong, Y. H. Shin, and N. H. Lee, *Thin Solid Films* **435**, 179 (2003).